J Mater Sci (2017) 52:3402–3418

Unification of molecular NIR fluorescence and aggregation-induced blue emission via novel dendritic zinc phthalocyanines

Lin Pan[1], Kun Jia[1,*], Hongguo Shou[1], Xuefei Zhou[1], Pan Wang[1], and Xiaobo Liu[1,*]

[1] *Research Branch of Advanced Functional Materials, High Temperature Resistant Polymer and Composites Key Laboratory of Sichuan Province, School of Microelectronics and Solid-State Electronics, University of Electronic Science and Technology of China, Chengdu 610054, People's Republic of China*

Received: 2 September 2016
Accepted: 18 November 2016
Published online: 29 November 2016

ABSTRACT

In this work, novel dendritic zinc phthalocyanines showing both molecular NIR fluorescence and aggregation-induced emission characteristics have been successfully synthesized via a two-step reaction on the basis of bisphthalonitrile precursors with different electron donor–conjugation–acceptor (D–π–A) structures. The luminescent properties of the resultant dendritic zinc phthalocyanines were fully investigated in *N*, *N*-dimethylformamide (DMF) solution, in DMF/H_2O mixed solvent, in the solid state as well as polymethylmethacrylate composite film. The dendritic zinc phthalocyanines substituted with hydroquinone, naphthalenediol, or dihydroxybiphenyl moieties exhibited an unusual luminescence changes from highly near infrared (NIR) emitting in molecular state to strongly blue fluorescence in aggregated state as well as solid state, where the maximum fluorescent emission wavelength and highest quantum yield were detected from dendritic zinc phthalocyanines containing naphthalenediol and dihydroxybiphenyl groups, respectively. On the contrary, dendritic zinc phthalocyanines bearing diphenylmethane or bisphenol A units only exhibit NIR fluorescent emission in their molecular state. The distinct fluorescent emissions for these dendritic zinc phthalocyanines are rationalized in the framework of molecular configuration and electron density distribution as clarified by density functional theory (DFT) calculation. Moreover, the well-organized three-dimensional microspheres composed of abundant rod-like building blocks were discovered via the self-assembly of dendritic zinc phthalocyanine molecules in DMF/H_2O (50/50 vol%) mixture.

Address correspondence to E-mail: jiakun@uestc.edu.cn; liuxb@uestc.edu.cn

DOI 10.1007/s10853-016-0628-7

Introduction

Organic fluorescent materials have attracted enormous attention in many fields ranging from biological imaging [1, 2], chemical sensors [3], and optoelectronic devices [4] mainly because of their excellent properties including versatile synthetic tailorability and high fluorescence quantum yield. Generally, the conventional organic fluorophores should be used in their dilute solution, since their fluorescent emission would be declined or even fully quenched when they were aggregated or existed in solid state, resulting to the so-called notorious aggregation-caused quenching (ACQ) effect, which is mainly resulted from the formation of non-photoactive species (excimers, H-type aggregates, etc.) [5, 6]. Thus, the ACQ effect of organic fluorophores would strongly hinder their potential applications in fluorescent bioprobes, data storage, chemical sensory systems, and organic light-emitting diodes (OLED) [7–12]. Therefore, many research groups have attempted to overcome these inherent disadvantages through chemical and physical approaches to improve the fluorescence quantum yield in aggregated and solid state.

In 2001, the Tang's team firstly reported the aggregation-induced emission (AIE) for the silole compound 1-methyl-1,2,3,4,5-pentaphenylsilole showing stronger fluorescence in the aggregated state compared to its molecular state in pure solution [13]. The AIE mechanism has been lately rationalized as the restriction of intramolecular rotation that normally dissipates energy of excited fluorophores via various non-radiation channels. Afterward, the tetraphenylethene, 8,8a-dihydrocyclopenta[α]indene, benzene-1,3,5-tricarboxamide, conjugated poly(diphenylacetylene)s, and other hexaphenylsilole derivatives were found with AIE characteristic and have been applied in many cutting edge fields, such as fluorescent pH sensors, biological DNA probes, polarized light emitters, and multi-responsive nanomaterials [14–18]. Thanks to these flourishing applications, increasing efforts have been devoted to design and synthesize enhanced AIE fluorophores including BF_2 fluorescent dyes [19], 1,1-Dicyano-2,2-bis(4-dimethylaminophenyl)ethylene [20], 4,4′-(9-oxo-9H-fluorene-2,7-diyl)dibenzaldehyde [21], (1,3-dimethyl)barbituric acid-functionalized anthracenes [22], and α-cyanostilbene functionalized tetraphenyl imidazole derivatives [23]. However, the majority of these AIE fluorophores are non-luminescent in molecular state due to the presence of diverse non-radiative channels. Therefore, the exploration of new-type fluorophores that exhibit both molecular emission and AIE-enabled aggregated or solid-state fluorescence is of great importance for even wider practical applications.

Zinc phthalocyanines have attracted increasing interests and attentions in the photodynamic therapy, non-linear optoelectronic devices, sensitive chemosensors, and photocatalysis for visible-light-driven degradation of organic dyes, thanks to their rich photochemical and photophysical properties including near-infrared emission, high singlet oxygen generation efficiency, and excellent photostability [24–31]. In the above-mentioned applications, a larger number of chemical protocols were utilized to synthesize soluble and non-aggregated zinc phthalocyanine complexes, mainly because of the fact that aggregated zinc phthalocyanines show attenuated or completely quenched optical properties [32–35]. Specifically, the reason for the quenched luminescence of zinc phthalocyanines was attributed to the formation of less emissive species including delocalized excimers or excitons upon aggregation. Meanwhile, photoluminescent properties for zinc phthalocyanine molecules have been hardly investigated in the solid state or in thin films.

In this work, we reported a series of dendritic zinc phthalocyanines showing both molecular emission and AIE-enabled aggregated or solid-state fluorescence, and their chemical structures, photophysical properties, intramolecular charge transfers, as well as morphology of self-assembling superstructures were fully characterized.

Experimental

Materials

4-nitrophthalonitrile, hydroquinone, 2, 6-naphthalenediol, 4, 4′-dihydroxybiphenyl, 4, 4′-dihydroxydiphenylmethane, and bisphenol A were obtained from Adamas Reagent Co. Ltd (Shanghai, China), while anhydrous potassium carbonate, zinc chloride, ammonium molybdate, dimethyl sulfoxide, methanol, acetone, ethanol, dimethylacetamide, and *N*, *N*-dimethylformamide were received from Kelong Reagent Co. Ltd (Chengdu, China). The polymethyl methacrylate (PMMA) was obtained from Titan

Scientific Co. Ltd (Shanghai, China). All the chemical materials were used as received without any further purification.

Measurements

Fourier transform infrared spectra of the prepared compounds were characterized with Shimadzu 8400S spectrometer. NMR spectra were obtained with a Bruker AV II-400 spectrometer. The ^{1}H-NMR (400 MHz) chemical shifts were measured relative to DMSO-d_6 (H: $\delta = 2.50$ ppm) as the internal references. Elemental analyses were performed by a Vario EL microelemental analyzer. The weight average molecular weight (M_w), number average molecular weight (M_n), and polydispersity index (M_w/M_n) were measured with gel permeation chromatography (PL-GPC220, Agilent). The melting temperature (T_m) of the synthesized compounds was tested with a TA Instruments DSC-Q100 at a heating rate of 20 °C min^{-1}. Thermal gravimetric analysis (TGA) of the prepared samples was conducted with a TA Instrument TGA-Q50 at a heating rate of 20 °C min^{-1}. The UV–Vis absorption spectra for dendritic zinc phthalocyanines in DMF solution and DMF/H_2O mixed solvent were recorded using a Persee TU 1901 UV–Vis spectrophotometer. The fluorescence excitation and emission spectra of dendritic zinc phthalocyanines in DMF solvent, in DMF/H_2O mixed solution, as well as in the solid state were obtained using a fluorescence spectrophotometer (F-4600, Hitachi). The scanning electron microscope (JSM-6490LV, JEOL) was utilized to obtain the self-assembling microstructure of dendritic zinc phthalocyanines in DMF/H_2O (50/50 vol%) mixed solution and surface morphology of the prepared polymer composite film. The fluorescence images were recorded with a fluorescent microscope (DP80, Olympus). The photos of sample vials under UV light were captured using a DSLR camera (D7000, Nikon).

Synthesis

The synthetic route and chemical structures of the compounds **2A–2E** and dendritic zinc phthalocyanines **3A–3E** are shown in Scheme 1. The specific procedure was demonstrated in the following.

Synthesis of compounds 2A–2E

The mixture containing compound **1** (2.9 mmol), 4-nitrophthalonitrile (1.00 g, 5.8 mmol), and anhydrous potassium carbonate (K_2CO_3) (0.90 g, 6.5 mmol) in 15 mL dimethyl sulfoxide (DMSO) solution was stirred at room temperature for 24 h under nitrogen atmosphere. The thermal transition and chemical structures of the compounds were characterized using DSC, FTIR, and ^{1}H-NMR spectra as well as elemental analyses. The DSC curves of the synthesized compounds **2A–2E** are shown in Fig. S1 in Electronic Supplementary Information (ESI).

Compound 2A

The reaction mixture was poured into H_2O, and the precipitate was washed with H_2O for three times and hot methanol for two times. The pure product was dried under vacuum for 12 h to obtain white powder. Yield: 0.75 g, 71.4%. T_m: 260.4 °C. ^{1}H-NMR [DMSO-d_6, 400 MHz, δ (ppm)]: 8.14 (*d*, $J = 8.8$ Hz, 2H, $-C_6H_3$), 7.88 (*d*, $J = 2$ Hz, 2H, $-C_6H_3$), 7.53–7.51 (*m*, 2H, $-C_6H_3$), 7.34 (*s*, 4H, $-C_6H_4$). IR (KBr, cm^{-1}): 3108, 3077, 3049, 2233, 1596, 1562, 1498, 1482, 1285, 1248, 1191, 1091, 1016. Anal.Calcd. (%) for $C_{22}H_{10}N_4O_2$: C 72.92; H 2.78; N 15.46; found: C 72.92; H 2.82; N 15.35.

Compound 2B

The reaction mixture was poured into H_2O, and the precipitate was washed with H_2O for three times, acetone for two times, and hot methanol for two times. The pure product was dried under vacuum for 12 h to obtain white powder. Yield: 0.93 g, 77.4%. T_m: 266.9 °C. ^{1}H-NMR [DMSO-d_6, 400 MHz, δ (ppm)]: 8.14 (*d*, $J = 8.8$ Hz, 2H, $-C_6H_3$), 8.07 (*d*, $J = 8.8$ Hz, 2H, $-C_{10}H_6$), 7.90 (*s*, 2H, $-C_6H_3$), 7.82 (*s*, 2H, $-C_6H_3$), 7.50–7.44 (*t*, 4H, $-C_{10}H_6$). IR (KBr, cm^{-1}): 3112, 3078, 3044, 2234, 1592, 1566, 1492, 1414, 1380, 1308, 1282, 1256, 1208, 1145, 1109, 1085. Anal.Calcd. (%) for $C_{26}H_{12}N_4O_2$: C 75.72; H 2.93; N 13.59; found: C 75.80; H 2.90; N 13.53.

Compound 2C

The reaction mixture was poured into H_2O, and the precipitate was washed with H_2O for three times, acetone for two times, and hot methanol for two times. The pure product was dried under vacuum for 12 h to obtain white powder. Yield: 0.98 g, 76.8%. T_m:

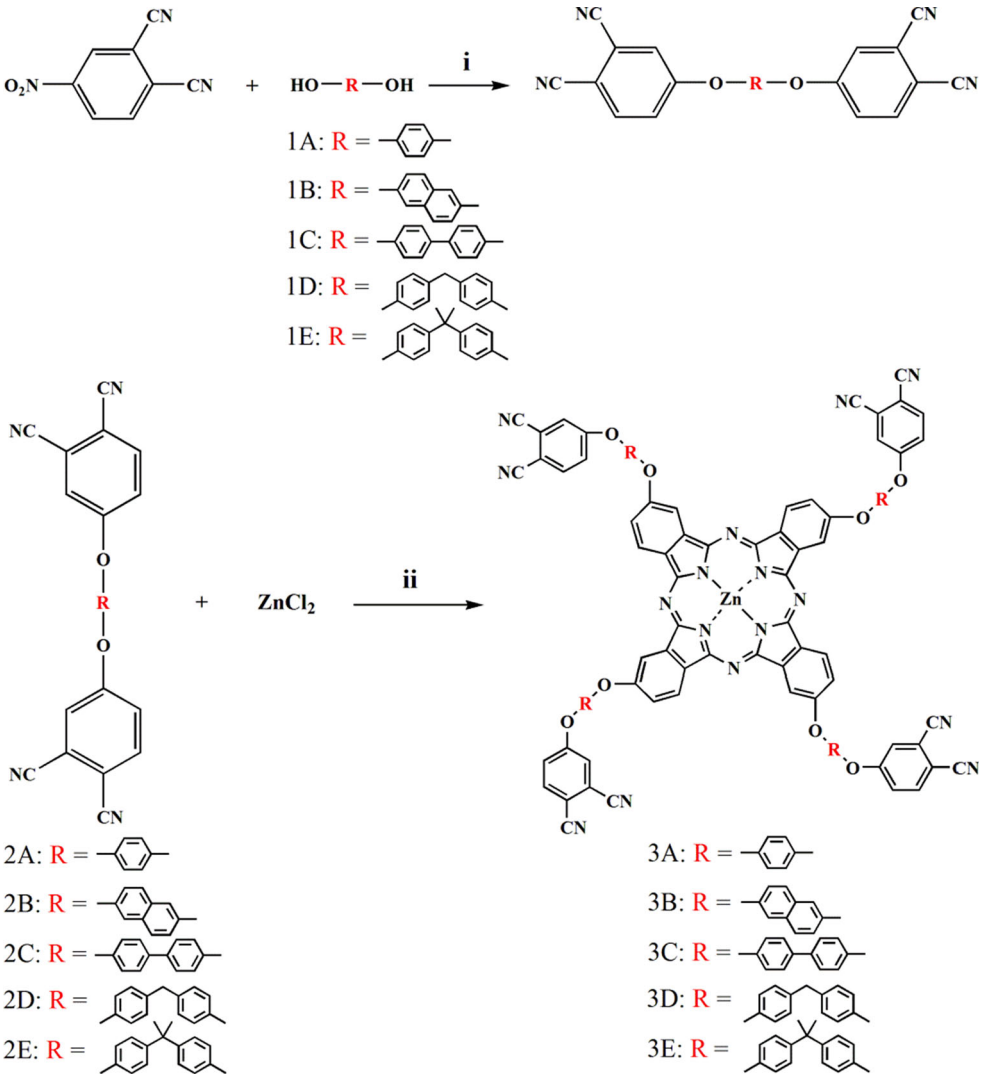

Scheme 1 Synthetic route and chemical structures of the targeted compounds. Synthetic condition: (*i*) K_2CO_3, DMSO, room temperature; (*ii*) ammonium molybdate, DMAC, reflux.

234.6 °C. ^{1}H-NMR [DMSO-d_6, 400 MHz, δ (ppm)]: 8.13 (*d*, J = 8.8 Hz, 2H, –C_6H_3), 7.87 (*d*, J = 2 Hz, 2H, –C_6H_3), 7.82 (*d*, J = 8.4 Hz, 4H, –$C_{12}H_8$), 7.47–7.45 (*m*, 2H, –C_6H_3), 7.31 (*d*, J = 8.4 Hz, 4H, –$C_{12}H_8$). IR (KBr, cm^{-1}): 3109, 3075, 3039, 2233, 1592, 1489, 1417, 1384, 1317, 1285, 1252, 1205, 1159, 1090, 1007. Anal.Calcd. (%) for $C_{28}H_{14}N_4O_2$: C 76.70; H 3.22; N 12.78; found: C 77.05; H 3.18; N 12.72.

Compound **2D**

The reaction mixture was poured into H_2O, and the precipitate was washed with H_2O for three times, alcohol for two times, and hot methanol for two times. The pure product was dried under vacuum for 12 h to obtain white powder. Yield: 1.15 g, 87.7%. T_m: 196.5 °C. ^{1}H-NMR [DMSO-d_6, 400 MHz, δ (ppm)]: 8.08 (*d*, J = 8.8 Hz, 2H, –C_6H_3), 7.78 (*s*, 2H, –C_6H_3), 7.37 (*t*, 6H, Ar–H), 7.14 (*d*, J = 8.0 Hz, 4H, –C_6H_4), 4.05 (*s*, 2H, –CH_2–). IR (KBr, cm^{-1}): 3080, 3040, 2927, 2232, 1592, 1565, 1501, 1484, 1418, 1286, 1278, 1250, 1202, 1167, 1094, 1017. Anal.Calcd. (%) for $C_{29}H_{16}N_4O_2$: C 76.98; H 3.56; N 12.38; found: C 76.90; H 3.60; N 12.52.

Compound **2E**

The reaction mixture was poured into H_2O, and the precipitate was washed with H_2O for three times, alcohol for two times, and hot methanol for two times. The pure product was dried under vacuum for 12 h to obtain white powder. Yield: 1.22 g, 87.6%. T_m: 196.5 °C. ^{1}H-NMR [DMSO-d_6, 400 MHz, δ (ppm)]: 8.10 (*d*, J = 8.8 Hz, 2H, –C_6H_3), 7.80 (*s*, 2H, –C_6H_3), 7.37 (*d*, J = 8.4 Hz, 6H, Ar–H), 7.13 (*d*, J = 8.4 Hz, 4H,

–C_6H_4), 1.69 (*s*, 6H, –CH_3). IR (KBr, cm^{-1}): 3108, 3075, 3046, 2975, 2233, 1590, 1561, 1503, 1489, 1421, 1305, 1289, 1256, 1211, 1178, 1083, 1016. Anal.Calcd. (%) for $C_{31}H_{20}N_4O_2$: C 77.49; H 4.20; N 11.66; found: C 77.60; H 4.15; N 11.59.

Synthesis of dendritic zinc phthalocyanines 3A–3E

A mixture of compound **2** (2 mmol), zinc chloride (0.068 g, 0.5 mmol), and ammonium molybdate (5 mg) in 20 mL of dimethylacetamide (DMAC) was heated at reflux under stirring. After the reaction liquid color turned into light-green, the mixture was kept reflux for 4.0 h. Next, the reaction mixture was poured into H_2O, and the precipitate was washed with H_2O for three times, hot methanol for two times, and dried under vacuum for 12 h. The chemical structures of the dendritic zinc phthalocyanines were characterized using UV–Vis, GPC, FTIR, and ^{1}H-NMR spectra. The ^{1}H-NMR spectra of dendritic zinc phthalocyanines 3A–3E are displayed in Fig. S10 in ESI.

Dendritic zinc phthalocyanine 3A

light-green powder, yield: 0.27 g. 37.3%. ^{1}H–NMR [DMSO-d_6, 400 MHz, δ (ppm)]: 8.13 (*d*, $J = 8.8$ Hz, Pc–H), 7.88–7.83 (*m*, Pc–H), 7.41 (*d*, $J = 7.6$ Hz, Pc–H), 7.34–7.27 (*m*, –C_6H_4). IR (KBr, cm^{-1}): 2233, 1766, 1720, 1610, 1499, 1476, 1447, 1365, 1309, 1268, 1229, 1190, 1089, 1040. GPC (relative to polystyrene standards): $M_w = 1801$, $M_n = 1712$, $M_w/M_n = 1.05$. UV–Vis (DMF, nm): $\lambda_{max1} = 610$, $\lambda_{max2} = 679$.

Dendritic zinc phthalocyanine 3B

light-green powder, yield: 0.25 g, 30.3%. ^{1}H-NMR [DMSO-d_6, 400 MHz, δ (ppm)]: 8.14 (*d*, $J = 8.8$ Hz, Pc-H), 8.07 (*d*, $J = 8.4$ Hz, –$C_{10}H_6$), 7.90 (*d*, $J = 8.0$ Hz, Pc–H), 7.87–7.77 (*m*, Pc–H), 7.50–7.42 (*m*, –$C_{10}H_6$). IR (KBr, cm^{-1}): 2234, 1769, 1721, 1595, 1484, 1444, 1380, 1309, 1278, 1146, 1112, 1042. GPC (relative to polystyrene standards): $M_w = 1989$, $M_n = 1872$, $M_w/M_n = 1.06$. UV–Vis (DMF, nm): $\lambda_{max1} = 611$, $\lambda_{max2} = 680$.

Dendritic zinc phthalocyanine 3C

light-green powder, yield: 0.32 g, 36.5%. ^{1}H-NMR [DMSO-d_6, 400 MHz, δ (ppm)]: 8.13 (*d*, $J = 8.8$ Hz, Pc–H), 7.86 (*s*, Pc–H), 7.82 (*d*, $J = 7.6$ Hz, –$C_{12}H_8$), 7.47–7.41 (*m*, Pc–H), 7.30 (*d*, $J = 8.8$ Hz, –$C_{12}H_8$). IR (KBr, cm^{-1}): 2232, 1769, 1720, 1593, 1486, 1361, 1312, 1279, 1247, 1207, 1166, 1089, 1041, 1008. GPC (relative to polystyrene standards): $M_w = 2122$, $M_n = 2096$, $M_w/M_n = 1.01$. UV–Vis (DMF, nm): $\lambda_{max1} = 610$, $\lambda_{max2} = 678$.

Dendritic zinc phthalocyanine 3D

light-green powder, yield: 0.20 g, 22.1%. ^{1}H-NMR [DMSO-d_6, 400 MHz, δ (ppm)]: 8.08 (*d*, $J = 8.0$ Hz, Pc–H), 7.80 (*d*, $J = 9.6$ Hz, Pc–H), 7.37–7.32 (*m*, Ar–H), 7.19–7.12 (*m*, –C_6H_4), 4.03 (*s*, –CH_2–). IR (KBr, cm^{-1}): 2232, 1767, 1719, 1652, 1598, 1561, 1502, 1478, 1441, 1363, 1312, 1276, 1234, 1203, 1167, 1092, 1041. GPC (relative to polystyrene standards): $M_w = 2347$, $M_n = 2306$, $M_w/M_n = 1.02$. UV–Vis (DMF, nm): $\lambda_{max1} = 611$, $\lambda_{max2} = 680$.

Dendritic zinc phthalocyanine 3E

light-green powder, yield: 0.15 g, 15.6%. ^{1}H-NMR [DMSO-d_6, 400 MHz, δ (ppm)]: 8.09 (*d*, $J = 8.6$ Hz, Pc–H), 7.79 (*s*, Pc–H), 7.35 (*s*, Ar–H), 7.11 (*s*, –C_6H_4), 1.69 (*s*, –CH_3). IR (KBr, cm^{-1}): 2233, 1770, 1723, 1652, 1560, 1504, 1480, 1427, 1385, 1310, 1276, 1234, 1173, 1084, 1016. GPC (relative to polystyrene standards): $M_w = 2633$, $M_n = 2415$, $M_w/M_n = 1.09$. UV–Vis (DMF, nm): $\lambda_{max1} = 610$, $\lambda_{max2} = 681$.

Preparation of zinc phthalocyanine–polymer composite film

The polymethyl methacrylate (125 mg) was dissolved in THF solution (5.0 mL) by stirring at room temperature for 12 h. Then the DMF solution (1.0 mL) of dendritic zinc phthalocyanine **3A** at a concentration of 1.0 and 2.0 mg mL^{-1} was added into the PMMA/THF mixture (5.0 mL), respectively. Finally, zinc phthalocyanine–polymer composite films were prepared using a spinning coater (KW-4A, Chemat Technology) at a rotation rate of 4000 rpm for 30 s and dried under vacuum at 30 °C for 12 h.

Results and discussion

Synthesis

As shown in Scheme 1, the compounds **2A–2E** were successfully synthesized via a nucleophilic

Table 1 Electronic absorption, excitation, and emission spectral data of dendritic zinc phthalocyanines **3A–3E**

Fluorophore	Matrix	Q-band λ_{max}/(nm)[a]	Excitation λ_{Ex}/(nm)[b]	Emission λ_{Em}/(nm)[c]	Stokes shift Δ_{Stokes}/(nm)[d]
3A	DMF	679	365	439, 694	74, 329
	DMF/H_2O (50/50 vol%)	688	365	465	100
	Solid	–	365	467	102
3B	DMF	680	365	433, 695	68, 330
	DMF/H_2O (50/50 vol%)	690	365	491	126
	Solid	–	365	487	122
3C	DMF	678	365	443, 695	78, 330
	DMF/H_2O (50/50 vol%)	688	365	475	110
	Solid	–	365	468	103
3D	DMF	680	365	445, 695	80, 330
	DMF/H_2O (50/50 vol%)	687	365	–	–
	Solid	–	365	–	–
3E	DMF	681	365	438, 695	73, 330
	DMF/H_2O (50/50 vol%)	686	365	–	–
	Solid	–	365	–	–

$\Delta_{Stokes} = {}^{c}\lambda_{Em} - {}^{b}\lambda_{Ex}$

[a] Maximum wavelength recorded using UV–Vis spectrophotometer

[b,c,d] Maximum wavelength or data derived from fluorescence excitation/emission spectra

substitution reaction of 4-nitrophthalonitrile with compound **1A–1E** in the presence of anhydrous potassium carbonate as the alkaline catalyst in DMSO solvent at room temperature, respectively. The cycloaddition reaction of compounds **2A–2E** with zinc chloride using the ammonium molybdate as the catalyst in DMAC solution was utilized to prepare dendritic zinc phthalocyanines **3A–3E**. All the studied zinc phthalocyanines could be obtained successfully through two-step synthesis, and the chemical structures of the synthesized dendritic zinc phthalocyanines were fully characterized with ultraviolet–visible absorption, infrared spectroscopy, and hydrogen nuclear magnetic resonance spectroscopy as well as gel permeation chromatography.

Electronic absorption and fluorescence spectra

The electronic absorption of dendritic zinc phthalocyanines **3A–3E** exhibited representative Q-band absorption in the visible light region at around 600–700 nm in DMF solution, and the Q-band absorption spectral data of dendritic zinc phthalocyanines **3A–3E** are summarized in Table 1. The UV–Vis optical spectroscopy of dendritic zinc phthalocyanines in DMF solution is shown in Fig. S2 (using dendritic zinc phthalocyanine **3A** as an example). The dendritic zinc phthalocyanine **3A** showed an intense UV absorption peak at 275 nm (B-band) along with a characteristic absorbance peak in the range of 600–700 nm (see inset of Fig. S2). While the B-band around 200–400 nm is attributed to the a_{2u}–e_g transition, the typical Q-band corresponds to the π–π* (a_{1u}–e_g) transition of phthalocyanine rings from the highest occupied molecular orbital (HOMO) to the lowest unoccupied molecular orbital (LUMO) [36, 37].

Aggregation behavior of metallized phthalocyanine complexes was usually investigated because of the fact that photoactive properties of these complexes could be controlled through the change of molecular state from single monomer to dimer and highly ordered supramolecules. In this work, the aggregation behavior of dendritic zinc phthalocyanines at different concentrations in DMF solution was examined using dendritic zinc phthalocyanine **3A** as an example. As shown in Fig. 1, when the concentration increased from 0.05 to 0.60 mg mL^{-1},

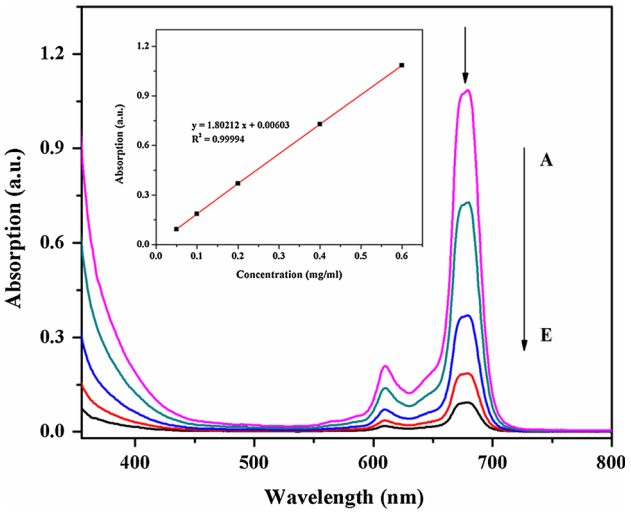

Figure 1 Aggregation behavior of the UV–Vis absorption spectra for dendritic zinc phthalocyanine **3A** using DMF as solvent at different concentrations: 0.60 (*A*), 0.40 (*B*), 0.20 (*C*), 0.10 (*D*), 0.05 (*E*) mg mL^{-1}. *Inset* Plot of absorbance at 679 nm versus concentration.

dendritic zinc phthalocyanine **3A** showed proportionally increased Q-band absorption at 600–700 nm region without any peak shift or distortion, meanwhile the linear Lambert–Beer law was observed from Q-band absorption intensity at 679 nm versus concentration of **3A** solution (see inset of Fig. 1), which demonstrated that dendritic zinc phthalocyanine aggregate was not formed at concentrations ranging from 0.05 to 0.60 mg mL^{-1}.

The fluorescence excitation and emission spectra of dendritic zinc phthalocyanines were recorded in DMF solution as shown in Fig. S3 (using dendritic zinc phthalocyanine **3A** as an example). It was observed that three fluorescent excitation peaks were detected at 365, 616, and 682 nm for dendritic zinc phthalocyanine **3A** through monitoring the fluorescent emission at 694 nm. The dendritic zinc phthalocyanine **3A** exhibited a sharp red emission peak at ~694 nm along with a broad blue emission at approximately 439 nm when the sample was excited at 365 nm, and it was clear that only single fluorescent emission peak at 694 nm was found under excitation at 616 nm and 682 nm. And the excitation and emission spectral data of dendritic zinc phthalocyanines **3B–3E** are fully summarized in Table 1. All the samples in DMF solution exhibited dual-emissive spectra at ~440 and ~695 nm as observed in Table 1, and the stokes shift of all dendritic zinc phthalocyanines was around 330 nm.

Fluorescence properties in the molecular state

The fluorescent properties of zinc phthalocyanines in the molecular state were dependent on the nature of the solution, the concentration, and the substituents. The dendritic zinc phthalocyanines **3A–3E** possessed good solubility in most organic solvents including dimethylformamide, dimethylacetamide,

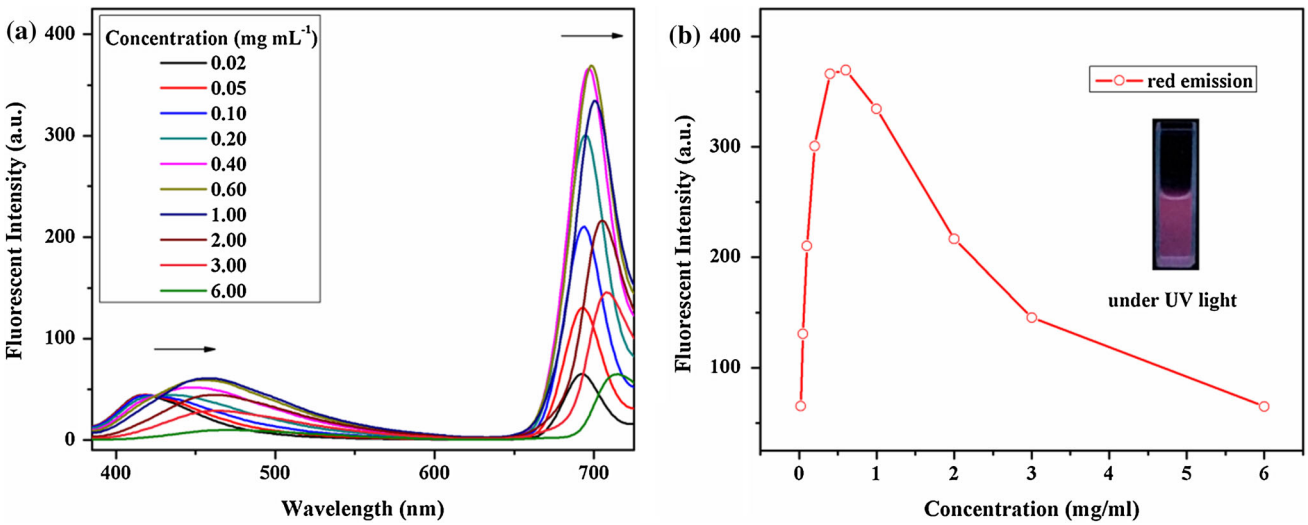

Figure 2 The fluorescence emission spectra of dendritic zinc phthalocyanine **3A** in DMF solution under excitation at 365 nm at different concentrations: 0.02, 0.05, 0.10, 0.20, 0.40, 0.60, 1.00, 2.00, 3.00, 6.00 mg mL^{-1} (**a**) and plot of red emission intensity versus concentration (**b**). *Inset* Image of sample under UV irradiation at 365 nm in DMF solution using a cuvette.

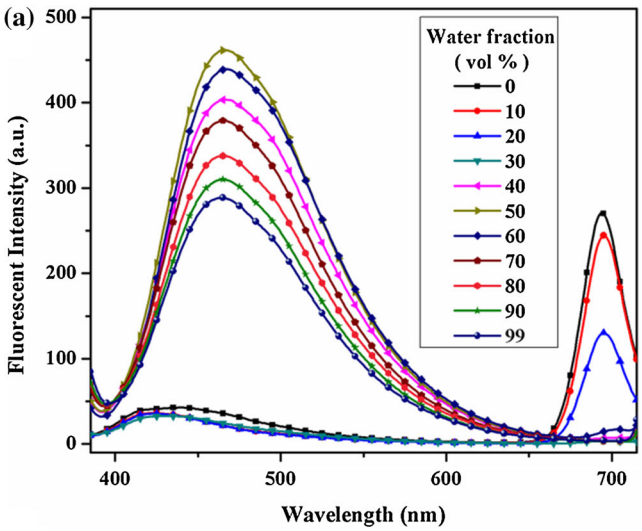
(a)
Water fraction
(vol %)
0
10
20
30
40
50
60
70
80
90
99
Fluorescent Intensity (a.u.)
Wavelength (nm)

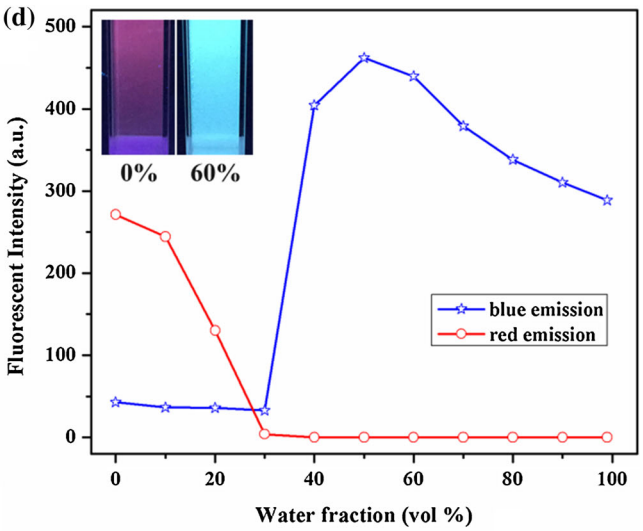
(d)
0%
60%
blue emission
red emission
Fluorescent Intensity (a.u.)
Water fraction (vol %)

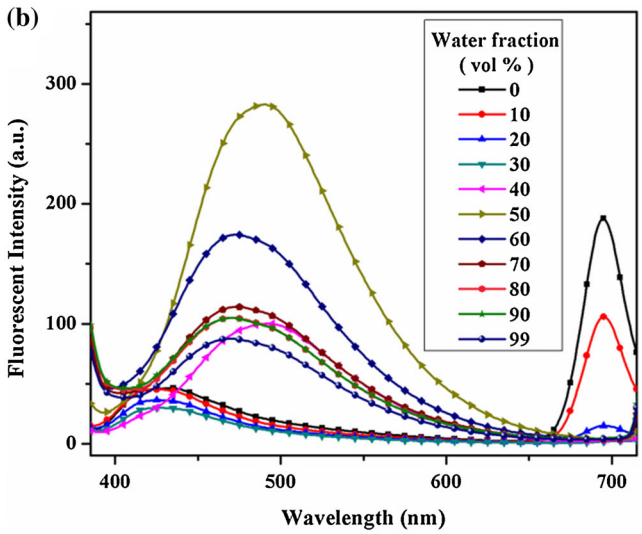
(b)
Water fraction
(vol %)
0
10
20
30
40
50
60
70
80
90
99
Fluorescent Intensity (a.u.)
Wavelength (nm)

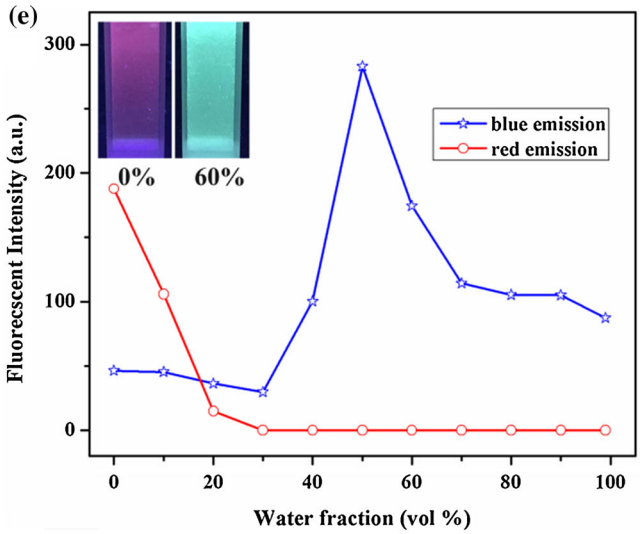
(e)
0%
60%
blue emission
red emission
Fluorescent Intensity (a.u.)
Water fraction (vol %)

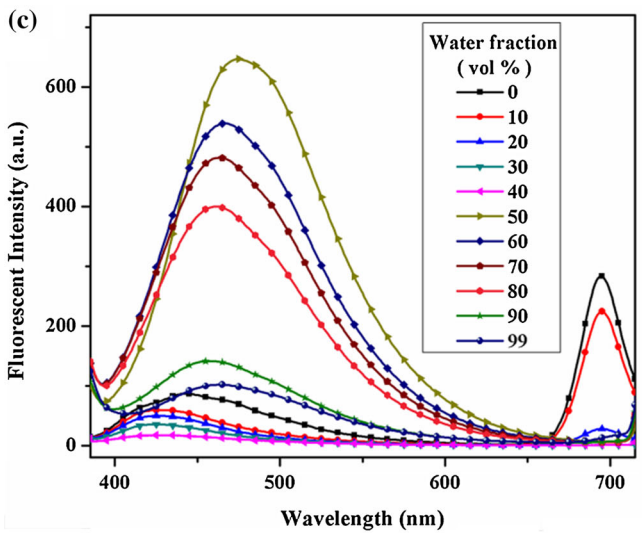
(c)
Water fraction
(vol %)
0
10
20
30
40
50
60
70
80
90
99
Fluorescent Intensity (a.u.)
Wavelength (nm)

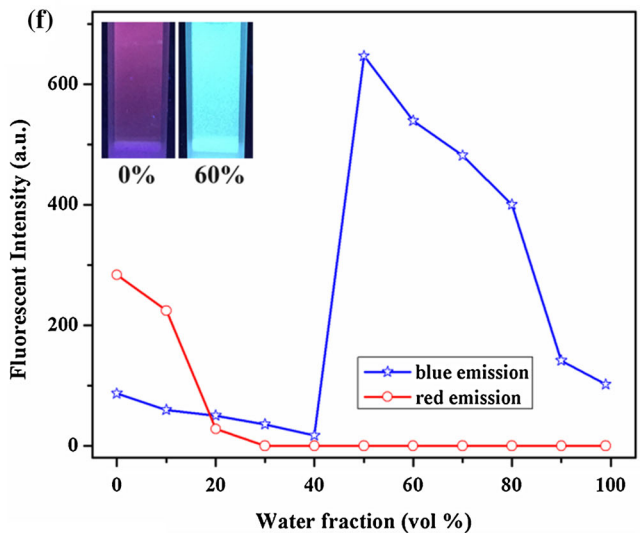
(f)
0%
60%
blue emission
red emission
Fluorescent Intensity (a.u.)
Water fraction (vol %)

◀**Figure 3** The fluorescence emission spectra of dendritic zinc phthalocyanines **3A** (**a**), **3B** (**b**), and **3C** (**c**) under excitation at 365 nm in DMF/H_2O mixture with different H_2O fractions and the plots of fluorescent emission intensity of dendritic zinc phthalocyanines **3A** (**d**), **3B** (**e**), and **3C** (**f**) versus the water fraction in the DMF/H_2O mixed solution.

dimethylsulfoxide, and pyridine as well as THF. Specifically, dendritic zinc phthalocyanine **3E** showed largest solubility in DMF when compared to other dendritic zinc phthalocyanines, which should be attributed to the more sterically demanding configuration presented in dendritic zinc phthalocyanine **3E**. The fluorescence emission spectra of dendritic zinc phthalocyanines at concentrations ranging from minimum concentration (0.02 mg mL^{-1}) to maximum concentration (6.00 mg mL^{-1}) are shown in Fig. 2 (using dendritic zinc phthalocyanine **3A** as an example). As seen in Fig. 2a, when the concentration increased, the red emission peak red-shifted ranging from 692 to 715 nm and blue band emission peak also red-shifted. This demonstrated that the concentration of dendritic zinc phthalocyanine 3A in DMF solution plays an important role for the location of fluorescent emission peak resulting from the formation of zinc phthalocyanine dimers. Figure 2b shows the plot of red emission intensity versus concentration; the maximum emission intensity was clearly observed when the concentration of dendritic zinc phthalocyanine **3A** was at ~0.40 mg mL^{-1} as displayed the image under UV light illumination in inset of Fig. 2b. The decreased red fluorescent emission intensity of dendritic zinc phthalocyanine **3A** at maximum concentration in DMF solution was clearly observed, and the photoluminescent intensity of the concentrated solution of dendritic zinc phthalocyanine **3A** was weak when compared to that of the dilute solvent, which implied that dendritic zinc phthalocyanine molecules under the condition of high concentration in DMF solution tend to form H-type (face to face) aggregation rather than J-type (head to tail) aggregation due to the combination of strong intermolecular π–π interactions and metal–ligand coordination bonding [38–41].

Fluorescence properties in the aggregated state

Similar to the conventional fluorophores, the fluorescence emission of dendritic zinc phthalocyanines **3D** and **3E** dispersed in DMF/H_2O mixed solution was obviously quenched compared to that recorded from DMF solution as displayed in Fig. S4. More specifically, the DMF solution of **3D** and **3E** was highly fluorescent with dual-emissive peaks at ~440 and 695 nm, and their emission intensity was obviously reduced when water was introduced into DMF solvent. The intensity of red fluorescence was so poor when water fraction was up to >30 vol% and blue emission was also attenuated, suggesting that abundant molecules of dendritic zinc phthalocyanines become aggregated. These results confirmed that the fluorescent emission of dendritic zinc phthalocyanines **3D** and **3E** was basically determined by the typical ACQ effect. Furthermore, the electronic absorption was used to probe the aggregation formation in DMF/H_2O mixed solution. The Q-band absorption at around 600–700 nm was red-shifted and became broader as shown in Fig. S4, which confirmed that zinc phthalocyanines might experience intense π–π interactions, leading to the formation of detrimental species that strongly quenched fluorescence [42].

Quite interestingly, we discovered that the fluorescent emission of dendritic zinc phthalocyanines **3A**, **3B**, and **3C** in DMF/H_2O solution can be modulated between ACQ and AIE-dominated framework, depending on the water fractions in mixed solution. As shown in Fig. 3, the intense sharp red emission at ~695 nm along with broad blue emission was obviously observed for dendritic zinc phthalocyanines **3A**, **3B**, and **3C** in pure DMF solvent, and the similar behavior was displayed for dendritic zinc phthalocyanines **3D** and **3E** (see Fig. S4). When the zinc phthalocyanines were dispersed in the DMF/H_2O mixed solvents where H_2O volume ratio was less than 30%, their red-emitting peak intensity was quenched as increasing of water quantity, which indicated the fluorescence of dendritic zinc phthalocyanines **3A**, **3B**, and **3C** were mainly determined by ACQ effect in this range. However, as more than 30% water was added to induce zinc phthalocyanine aggregation formation (see red-shift and broaden UV–Vis spectra shown in Fig. S5), it was clear from Fig. 3 that the blue-emissive peak for all these samples in the aqueous mixtures gradually appeared. The enhanced blue-emissive intensity was recorded by increasing water content, and a highest broad blue-emissive signal was obtained in 50 vol% aqueous mixture. These spectra data demonstrated that

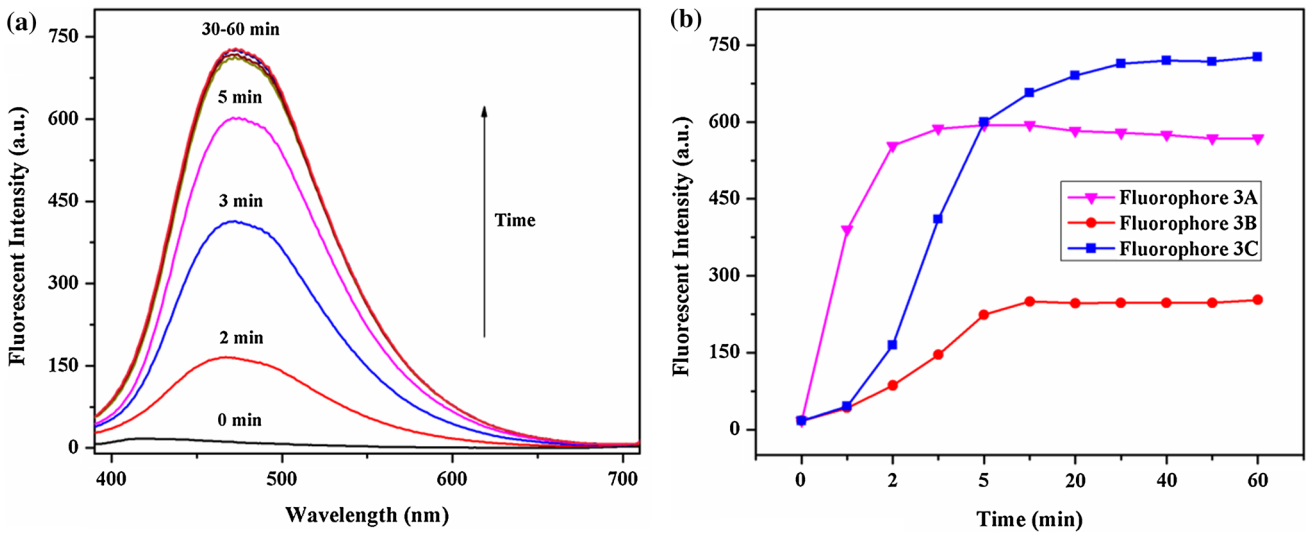

Figure 4 Aggregating time-dependent fluorescence emission spectrum for dendritic zinc phthalocyanine **3C** under excitation at 365 nm in DMF/H_2O (50/50 vol%) mixture (**a**) and plot of emission intensity for dendritic zinc phthalocyanines **3A–3C** versus aggregation time (**b**) under excitation at 365 nm.

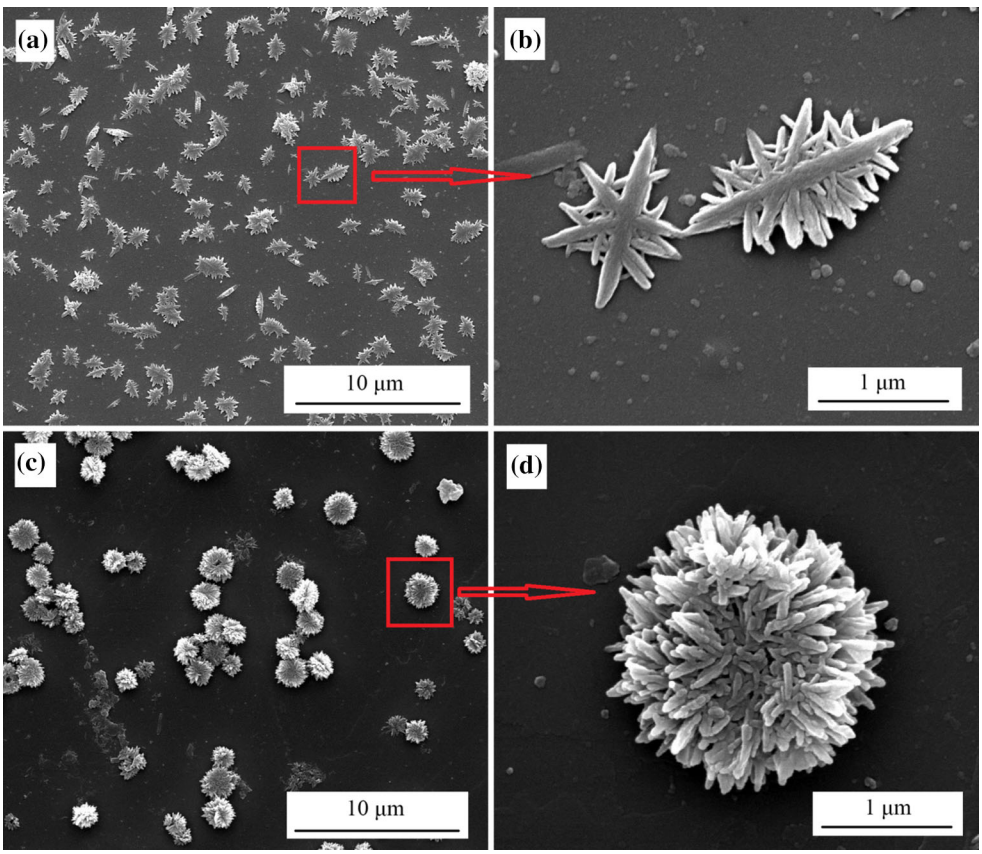

Figure 5 Dependence of self-assembled supramolecular structures for dendritic zinc phthalocyanine **3A** to aggregating time in DMF/H_2O (50/50 vol%) mixture: low-magnification SEM image (**a**) and high-magnification SEM image (**b**) of supramolecular structures at 60 s; low-magnification SEM image (**c**) and high-magnification SEM image (**d**) of supramolecular structures at 120 s.

dendritic zinc phthalocyanines **3A**, **3B**, and **3C** were typical blue AIE fluorophores. It was believed that the restriction of intramolecular rotation and strong π–π interactions were main reasons for the observed AIE enhancement. Afterward, the intensity of broad blue emission was again quenched when water fraction was higher than 50%, indicating that the ACQ again became the dominant factor for fluorescence of random zinc phthalocyanine aggregates generated via the fast precipitation process. Based on the above results, the fluorescent emission of dendritic zinc phthalocyanines **3A**, **3B**, and **3C** can be readily modulated from basically red emitting in molecular state to blue fluorescent in aggregated state.

To well understand the kinetics of the AIE effect for dendritic zinc phthalocyanines **3A–3C**, influence of the aggregating time on their fluorescence emission in DMF/H_2O (50/50 vol%) mixed solution was investigated. Equal volume of water was immediately added into the DMF solvent of dendritic zinc phthalocyanines to obtain the DMF/H_2O mixture. Next, the emission spectrum of the mixture was recorded using a fluorescence spectrophotometer at a specific time interval. As shown in Fig. 4a, the blue emission intensity of dendritic zinc phthalocyanine **3C** was enhanced drastically for the first 30 min, and reached a maximum emissive value thereafter. However, the maximum value of fluorescence emission for dendritic zinc phthalocyanine **3A** was obtained within 2 min as displayed in Fig. 4b. This demonstrated that intramolecular rotation of dendritic zinc phthalocyanine **3A** was restricted more rapidly when compared to **3C**, as the biphenyl groups of dendritic zinc phthalocyanine **3C** were larger than others and more time was required to enhance the restricted intramolecular rotation effects.

Furthermore, the surface morphology of zinc phthalocyanine supramolecular structures formed during aggregation process was characterized with SEM. Taking dendritic zinc phthalocyanine **3A** as an example, the well-organized self-assembled superstructures with different morphologies could be successfully formed. Specifically, equal volume of water was rapidly added into DMF solution of **3A,** and the resulted mixture of phthalocyanine aggregates was kept at room temperature for 60 s, during which the two-dimensional (2D) microstructures were obtained as displayed in Fig. 5a. From the high-magnification SEM image (see Fig. 5b), it was clear that the 2D microstructure was a well-designed leaf-like supramolecular microstructure. We assumed that this leaf-like structure was developed via the following steps: a rigid rod-like building block was initially formed via self-assembly of zinc phthalocyanines, which served as the "seeds" for further growth of more rod-like molecules. Thus, it was assumed that the driven force for the rod-like microstructure formation was the combination of metal–ligand coordination bonding, intermolecular cyano interactions, and strong intermolecular π–π interactions [43]. More interestingly, when the aggregating time was prolonged to 120 s, the self-assembled three-dimensional (3D) microspheres could be successfully formed as observed in the low-magnification SEM image (see Fig. 5c). Furthermore, as shown in high-magnification SEM image of Fig. 5d, the self-assembled supramolecular aggregation was a well-organized 3D microsphere which was composed of abundant assembling rod-like building

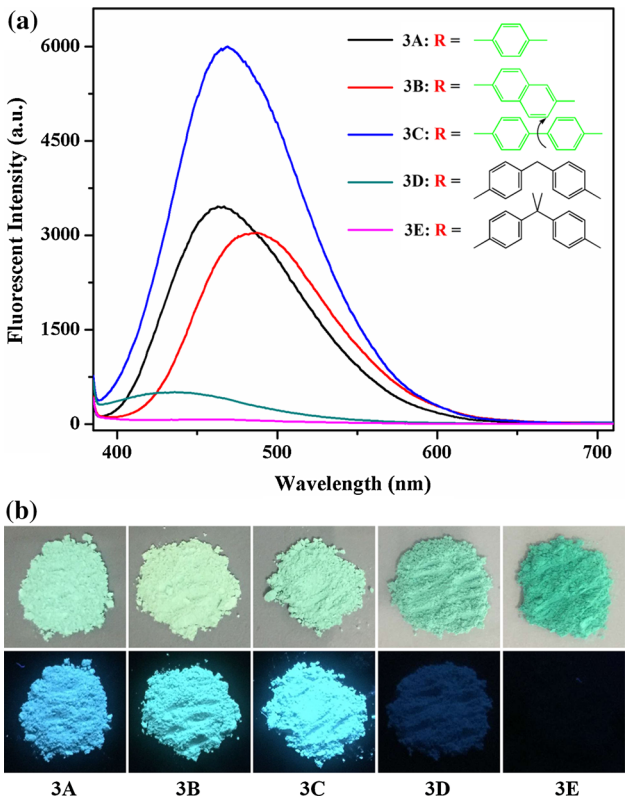

Figure 6 The fluorescence emission spectra of dendritic zinc phthalocyanines **3A–3E** in the solid state at an excitation wavelength of 365 nm (**a**) and the color of dendritic zinc phthalocyanines **3A-3E** in the solid state under visible light (*top*) and UV 365 nm (*down*) illumination (**b**).

blocks. Based on the obtained result from the fluorescence spectra as seen in Fig. 4, it could be concluded that the 3D microsphere was highly photoluminescent compared to the 2D leaf-like microstructure.

Fluorescence properties in the solid state

It is well known that conventional metallized phthalocyanines in the solid state exhibit non-photoluminescence properties mainly due to delocalized excimers or excitons leading to enhanced non-radiative deactivation [44]. However, dendritic zinc phthalocyanines **3A**, **3B**, and **3C** in this work showed attractive photoactive properties as displayed in Fig. S6. Two peaks at ~280 and 365 nm were detected from excitation spectra of dendritic zinc phthalocyanines **3A**, **3B**, and **3C** in the solid state, and the highest fluorescence emission intensity of dendritic zinc phthalocyanines could be obtained under excitation at 365 nm. As shown in Fig. 6, dendritic zinc phthalocyanine **3C** exhibited the maximum fluorescent emission intensity, and the emitting intensity of dendritic zinc phthalocyanine **3C** was nearly two-fold larger than that of dendritic zinc phthalocyanines **3A** and **3B**. The enhanced emission intensity of dendritic zinc phthalocyanine **3C** was likely owing to the biphenyl group presented in dendritic zinc phthalocyanine **3C**. The naphthalene-conjugated structure leads to the red-shifted emission wavelength of dendritic zinc phthalocyanine **3B** (*c*. 487 nm) in the solid state when compared to that of dendritic zinc phthalocyanines **3A** (465 nm) and **3C** (468 nm). Meanwhile, it can be obviously observed that dendritic zinc phthalocyanines containing diphenylmethane or bisphenol A units (**3D** and **3E**) in the solid state showed quite weak fluorescence emission in the visible light region, which might be attributed to the flexible structure of the diphenylmethane and bisphenol A units resulting in the free intramolecular rotation effects. The color of dendritic zinc phthalocyanines **3A–3D** was light-

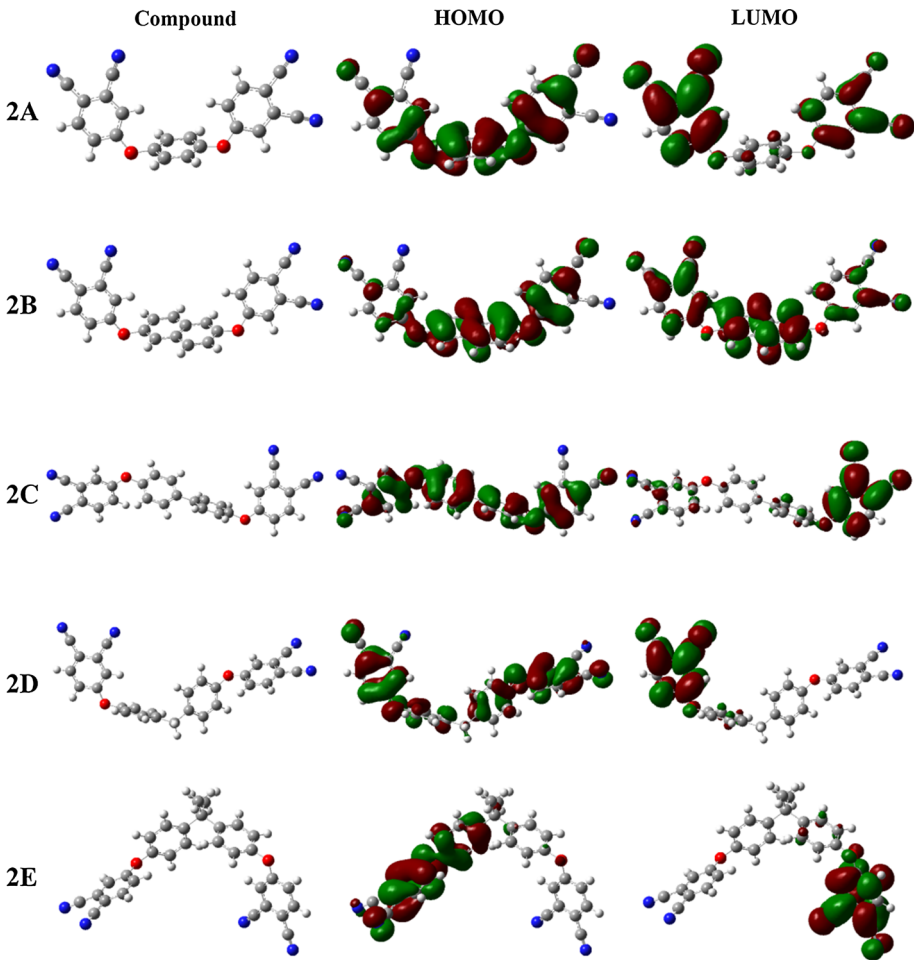

Figure 7 The frontier molecular orbitals of compounds **2A–2E** (the geometry was optimized at the hybrid B3LYP level using the split valence 6-31G basis set).

Table 2 Thermal properties of dendritic zinc phthalocyanines **3A–3E**

Fluorophore	T_5% (°C)	T_{10}% (°C)	Char yield (%) at 600 °C
3A	373.86	387.48	45.53
3B	382.93	399.72	67.04
3C	396.61	412.75	61.53
3D	388.57	439.15	73.63
3E	357.62	409.15	63.94

green, while **3E** exhibited green under visible light illumination as shown in Fig. 6b. Under UV lamp excitation (365 nm), dendritic zinc phthalocyanine **3A** was authentic blue and green color was detected from **3B**. Moreover, dendritic zinc phthalocyanine **3C** showed highest luminescence which could be confirmed by the fluorescence spectrum.

It has been believed that the solid-state fluorescence properties of dendritic zinc phthalocyanines **3A–3E** have a close relationship with the chemical structure of their corresponding precursor compounds **2A–2E** according to our best knowledge. Therefore, the density functional theory (DFT) calculations were carried out at the hybrid B3LYP level using the split valence 6-31G basis set to simulate the optimized molecular configuration and charge transfer process. The data obtained from DFT calculations including HOMO energy, LUMO energy, and HOMO–LUMO energy gap are fully summarized in Table S1. The optimized molecular configuration and the electron density distribution of the HOMO and LUMO levels for compounds **2A–2E** are shown in Fig. 7. It was clearly observed that molecular structures of compounds **2A**, **2B**, and **2C** showed better planarity in comparison to that of compounds **2D** and **2E** resulting in the easier charge transfer from the HOMO to the LUMO, and the charge transfer of compound **2C** was enhanced compared to that of compounds **2A** and **2B**, which should be due to the presence of longer conjugation bridge of biphenyl. The enhanced charge transfer of compound **2C** would normally contribute to an easier electron

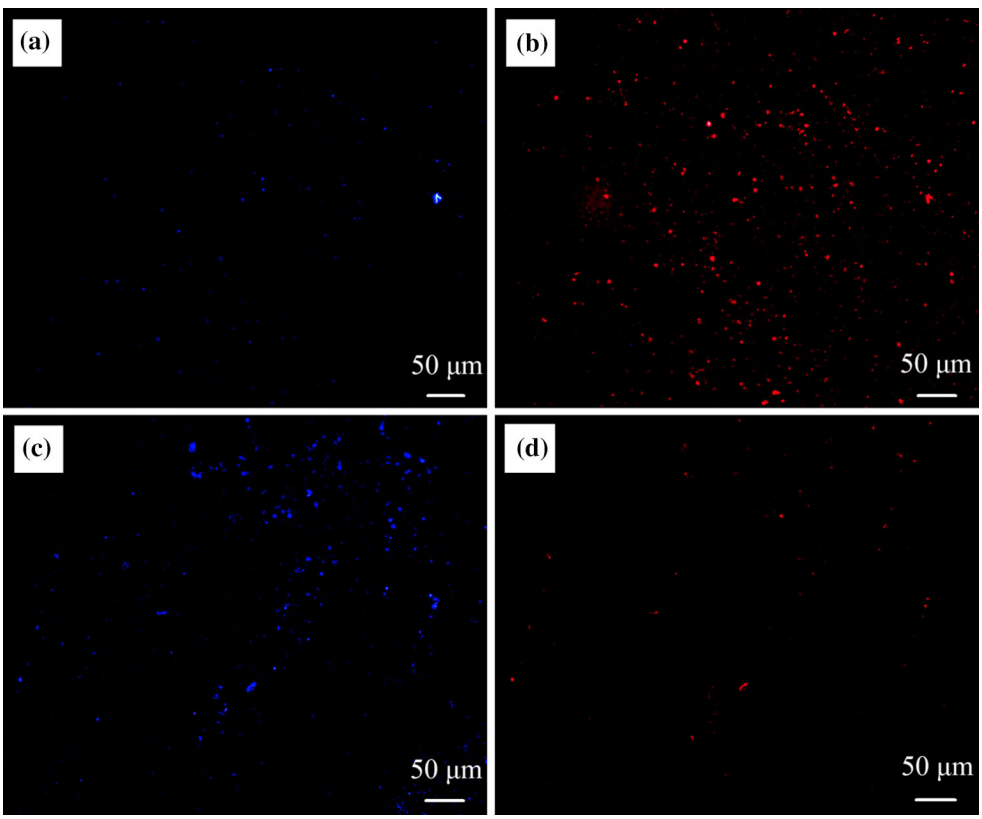

Figure 8 Concentration-dependent luminescent behavior of dendritic zinc phthalocyanine **3A** in the polymer composite film: low-concentration image (**a**) and high-concentration image (**c**) *under* the *blue* channel; low-concentration image (**b**) and high-concentration image (**d**) *under* the *red* channel.

transition, which in turn leads to its increased luminescence. Meanwhile, the lowest HOMO–LUMO energy gap of 4.287 eV was recorded for compound **2B** as shown in Table S1, which was well correlated with the largest fluorescent emission wavelength of dendritic zinc phthalocyanine **3B**. Interestingly, compounds **2D** and **2E** displayed totally different electron density distribution compared with those of compounds **2A**, **2B**, and **2C**. More specifically, the electrons, uniformly dispersed in the overall molecule of **2D** at ground state, were obviously transferred to the phthalonitrile moiety with strong electron-withdrawing ability upon photoexcitation, and the charge transfer process from HOMO to LUMO was further enhanced for **2E**. The nearly "total charge transfer" for **2D** and **2E** should be attributed to the presence of electron-donating groups (methylene and propyl), which would promote the photo-induced electron transfer process that strongly quenches their luminescence.

Thermal stability of metallized phthalocyanines is important for their practical applications; thus, the thermal properties of dendritic zinc phthalocyanines **3A–3E** were evaluated by the TGA analysis as shown in Fig. S7, and the detail data from the TGA curves are listed in Table 2. All dendritic zinc phthalocyanines **3A–3E** exhibited good thermal stability, and the temperatures corresponding to 5wt% weight loss (T_5%) are higher than 350 °C. The maximum value of T_5% was detected from dendritic zinc phthalocyanine **3C** (396.61 °C), which would be attributed to molecular structure of compound **2C**. However, the T_5% value was lowest for dendritic zinc phthalocyanine **3E** (357.62 °C) mainly owing to the destruction of rigid construction and conjugated degree by propyl group.

Fluorescent images of zinc phthalocyanine–polymer composite film

As discussed previously, the luminescent properties of dendritic zinc phthalocyanines **3A–3C** can be well modulated from molecular state to aggregated state and solid state. Therefore, the experimental

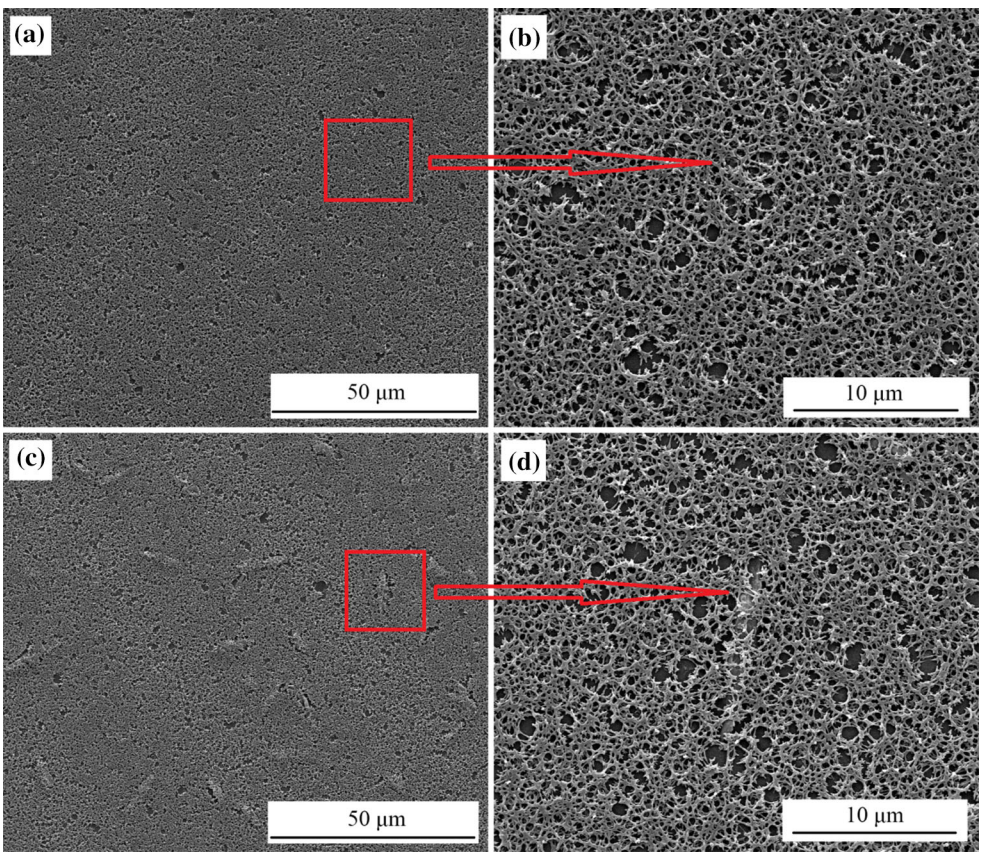

Figure 9 The SEM images of dendritic zinc phthalocyanine **3A** in the polymer composite film: low-concentration image (**a** and **b**) and high-concentration image (**c** and **d**).

investigations of polymer composite film with different concentrations of zinc phthalocyanines are of great interests. In this work, PMMA solution containing different concentrations of dendritic zinc phthalocyanines (using dendritic zinc phthalocyanine **3A** as an example) was spin coated to fabricated flexible fluorescent film. As displayed in Fig. S8, the small particles were clearly observed and well dispersed from low-concentration sample, while vast rod-like structures were found and local regions have abundant rod-like structures in high-concentration image. It was believed that the small particle and rod-like structure were attributed to the nanoassembles of zinc phthalocyanine molecules. For polymer composite film containing lower concentration of **3A**, the weak blue-emitting fluorescence and intense red fluorescence were detected from fluorescent microscope images (see Fig. 8a, b), while for polymer composite film doping with higher content **of 3A**, the intense blue fluorescence along with quenched red emission was observed due to the presence of zinc phthalocyanine aggregates (see Fig. 8c, d). These results demonstrated that the luminescent behavior of zinc phthalocyanine–polymer composite film could be readily modulated by controlling the doping concentration of zinc phthalocyanines, which was similar to the emissive spectra of dendritic zinc phthalocyanines in DMF/H_2O mixed solution.

The surface morphology of zinc phthalocyanine–polymer composite film has been investigated utilizing a scanning electron microscope. It can be seen that the polymer composite film displayed outstanding transmittance because of their loose network structures. Meanwhile, the luminescence properties of dendritic zinc phthalocyanines were not almost influenced after introducing the PMMA into THF/DMF mixed solvent (see Fig. S9). As shown in Fig. 9a, b, zinc phthalocyanine molecular aggregates were not found for the polymer composite film with a low concentration of dendritic zinc phthalocyanines. On the contrary, abundant assembling rod-like microstructures had been detected from the polymer composite film with a high concentration of dendritic zinc phthalocyanines as visualized in Fig. 9c. It was clear that a rod-like microstructure was embedded in the loose network structure of PMMA observed in Fig. 9d. The results assumed that the PMMA plays an important character about the formation of dendritic zinc phthalocyanine aggregation.

Conclusions

In conclusion, we designed and synthesized a new family of fluorophores based on dendritic zinc phthalocyanines that can emit strongly in molecular, aggregated, solid states as well as in polymer composite films. Specifically, dendritic zinc phthalocyanines **3A–3C** exhibited enhanced blue-emitting luminescence in comparison to typical ACQ characteristics of dendritic zinc phthalocyanines **3D–3E** upon their aggregation. More interestingly, novel dendritic zinc phthalocyanines **3A–3C** showed an interesting change from highly NIR emitting in molecular state to strongly blue fluorescence in aggregated state. Aggregating time-dependent fluorescence emission and self-assembling supramolecular microstructures in 50 vol% aqueous mixture were fully investigated, and a well-organized self-assembled aggregation including 3D microsphere and 2D leaf-like microstructure for dendritic zinc phthalocyanine **3A** could be successfully obtained. Meanwhile, these dendritic zinc phthalocyanines **3A–3C** displayed solid-state luminescence, and their solid-state fluorescence was rationalized in terms of molecular configuration and charge transfer as clarified by the DFT calculations. Moreover, dendritic zinc phthalocyanine-doped PMMA polymer composite films were prepared via a simple approach, and their luminescent behaviors were systematically explored. Based on the above results, we believed that dendritic zinc phthalocyanines **3A–3C** could find potential applications in high-tech fields of biological imaging agents, fluorescent chemosensor, as well as flexible optoelectronic devices.

Acknowledgements

The authors acknowledge the financial support from the National Natural Science Foundation of China (Project Nos. 51373028, 51403029), the Scientific Research Foundation for the Returned Overseas Chinese Scholars from State Education Ministry, South Wisdom Valley Innovative Research Team Program, and Ningbo Major Science and Technology Research Plan (2013B06011).

Electronic supplementary material: The online version of this article (doi:10.1007/s10853-016-0628-7)

contains supplementary material, which is available to authorized users.

References

[1] Mandal K, Jana D, Ghorai BK, Jana NR (2016) Fluorescent imaging probe from nanoparticle made of AIE molecule. J Phys Chem C 120:5196–5206

[2] Yin W, Zhu H, Wang R (2014) A sensitive and selective fluorescence probe based fluorescein for detection of hypochlorous acid and its application for biological imaging. Dyes Pigments 107:127–132

[3] Zhu X, Lin Q, Chen P, Fu YP, Zhang YM, Wei TB (2016) A novel pH sensor which could respond to multi-scale pH changes via different fluorescence emissions. New J Chem 40:4562–4565

[4] Shi H, Xin D, Bai SD et al (2016) The synthesis, crystal structures, aggregation-induced emission and electroluminescence properties of two novel green-yellow emitters based on carbazole-substituted diphenylethene and dimesitylboron. Org Electron 33:78–87

[5] Thomas SW, Joly GD, Swager TM (2007) Chemical sensors based on amplifying fluorescent conjugated polymers. Chem Rev 107:1339–1386

[6] Yuan WZ, Lu P, Chen S et al (2010) Changing the behavior of chromophores from aggregation-caused quenching to aggregation-induced emission: development of highly efficient light emitters in the solid state. Adv Mater 22:2159–2163

[7] Song QH, Wu QQ, Liu CH, Du XJ, Guo QX (2013) A novel fluorescent probe for selective detection of thiols in acidic solutions and labeling of acidic organelles in live cells. J Mater Chem B 1:438–442

[8] Lee IH, Song W, Lee JY (2016) Aggregation-induced emission type thermally activated delayed fluorescent materials for high efficiency in non-doped organic light-emitting diodes. Org Electron 29:22–26

[9] Lei Y, Li H, Gao W et al (2014) Highly sensitive conjugated polymer fluorescent sensors based on benzochalcogendiazole for nickel ions in real-time detection. J Mater Chem C 2:7402–7410

[10] Wang Y, Liu W, Bu L et al (2013) Reversible piezochromic luminescence of 9,10-bis[(N-alkylcarbazol-3-yl)vinyl]anthracenes and the dependence on N-alkyl chain length. J Mater Chem C 1:856–862

[11] Liu Y, Tao X, Wang F et al (2008) Aggregation-induced emissions of fluorenonearylamine derivatives: a new kind of materials for nondoped red organic light-emitting diodes. J Phys Chem C 112:3975–3981

[12] Zhao Z, Chen S, Lam JWY et al (2010) steric hindrance, electronic communication, and energy transfer in the photo—and electroluminescence processes of aggregation-induced emission luminogens. J Phys Chem C 114:7963–7972

[13] Luo J, Xie Z, Lam JWY et al (2001) Aggregation-induced emission of 1-methyl-1,2,3,4,5-pentaphenylsilole. Chem Commun 18:1740–1741

[14] Hong Y, Lam JWY, Tang BZ (2009) Aggregation-induced emission: phenomenon, mechanism and applications. Chem Commun 29:4332–4353

[15] Hong Y, Lam JWY, Tang BZ (2011) Aggregation-induced emission. Chem Soc Rev 40:5361–5388

[16] Zhao N, Lam JWY, Sung HHY et al (2014) Effect of the counterion on light emission: a displacement strategy to change the emission behaviour from aggregation-caused quenching to aggregation-induced emission and to construct sensitive fluorescent sensors for Hg^{2+} detection. Chem Eur J 20:133–138

[17] Kwok RTK, Leung CWT, Lam JWY, Tang BZ (2015) Biosensing by luminogens with aggregation-induced emission characteristics. Chem Soc Rev 44:4228–4238

[18] Zhang Y, Li J, Tang BZ, Wong KS (2014) Aggregation enhancement on two-photon optical properties of AIE-Active D-TPE-A molecules. J Phys Chem C 118:26981–26986

[19] Zheng J, Huang F, Li Y et al (2015) The aggregation-induced emission enhancement properties of BF2 complex isatin-phenylhydrazone: synthesis and fluorescence characteristics. Dyes Pigments 113:502–509

[20] Botta C, Benedini S, Carlucci L et al (2016) Polymorphism-dependent aggregation induced emission of a push-pull dye and its multi-stimuli responsive behavior. J Mater Chem C 4:2979–2989

[21] Xu F, Wang H, Du X et al (2016) Structure, property and mechanism study of fluorenone-based AIE dyes. Dyes Pigments 129:121–128

[22] Yin G, Ma Y, Xiong Y, Cao X, Li Y, Chen L (2016) Enhanced AIE and different stimuli-responses in red fluorescent (1,3-dimethyl)barbituric acid-functionalized anthracenes. J Mater Chem C 4:751–757

[23] Zhang Y, Li H, Zhang G et al (2016) Aggregation-induced emission enhancement and mechanofluorochromic properties of [small alpha]-cyanostilbene functionalized tetraphenyl imidazole derivatives. J Mater Chem C 4:2971–2978

[24] Nyokong T (2007) Effects of substituents on the photochemical and photophysical properties of main group metal phthalocyanines. Coord Chem Rev 251:1707–1722

[25] Gao Z, Tao X, Cui Y, Satoh T, Kakuchi T, Duan Q (2011) Synthesis of end-functionalized poly(N-isopropylacrylamide) with group of asymmetrical phthalocyanine via atom

transfer radical polymerization and its photocatalytic oxidation of Rhodamine B. Polym Chem 2:2590–2596

[26] Zheng BY, Zhang HP, Ke MR, Huang JD (2013) Synthesis and antifungal photodynamic activities of a series of novel zinc(II) phthalocyanines substituted with piperazinyl moieties. Dyes Pigments 99:185–191

[27] Swain D, Singh R, Singh VK, Krishna NV, Giribabu L, Rao SV (2014) Sterically demanding zinc(II) phthalocyanines: synthesis, optical, electrochemical, nonlinear optical, excited state dynamics studies. J Mater Chem C 2:1711–1722

[28] Anaya-Plaza E, Oliva MM, Kunzmann A et al (2015) Quaternized pyridyloxy phthalocyanines render aqueous electron-donor carbon nanotubes as unprecedented supramolecular materials for energy conversion. Adv Funct Mater 25:7418–7427

[29] Venkatramaiah N, Rocha DMGC, Srikanth P, Almeida Paz FA, Tome JPC (2015) Synthesis and photophysical characterization of dimethylamine-derived Zn(II)phthalocyanines: exploring their potential as selective chemosensors for trinitrophenol. J Mater Chem C 3:1056–1067

[30] Wang A, Gui L, Lu S, Zhou L, Zhou J, Wei S (2016) Tumor microenvironment-responsive charge reversal zinc phthalocyanines based on amino acids for photodynamic therapy. Dyes Pigments 126:239–250

[31] Jia K, Pan L, Wang Z et al (2016) Morphology and photophysical properties of dual-emissive hyperbranched zinc phthalocyanines and their self-assembling superstructures. J Mater Sci 51:3191–3199. doi:10.1007/s10853-015-9630-8

[32] Durmuş M, Yaman H, Göl C, Ahsen V, Nyokong T (2011) Water-soluble quaternized mercaptopyridine-substituted zinc-phthalocyanines: synthesis, photophysical, photochemical and bovine serum albumin binding properties. Dyes Pigments 91:153–163

[33] Göl C, Durmuş M (2012) Investigation of photophysical, photochemical and bovine serum albumin binding properties of novel water-soluble zwitterionic zinc phthalocyanine complexes. Synth Met 162:605–613

[34] Liu W, Jensen TJ, Fronczek FR, Hammer RP, Smith KM, Vicente MGH (2005) Synthesis and cellular studies of nonaggregated water-soluble phthalocyanines. J Med Chem 48:1033–1041

[35] Dumoulin F, Durmuş M, Ahsen V, Nyokong T (2010) Synthetic pathways to water-soluble phthalocyanines and close analogs. Coord Chem Rev 254:2792–2847

[36] Zhang M, Shao C, Guo Z et al (2011) Highly efficient decomposition of organic dye by aqueous-solid phase transfer and in situ photocatalysis using hierarchical copper phthalocyanine hollow spheres. ACS Appl Mater Interfaces 3:2573–2847

[37] Nyokong T, Gasyna Z, Stillman MJ (1987) Analysis of the absorption and magnetic circular dichroism spectra of zinc phthalocyanine and the.pi.-cation-radical species [ZnPc(1-)].cntdot.+. Inorga Chem 26:1087–1095

[38] Zhang C, Jing L, Lin S et al (2013) Helical self-assembly of optically active phthalocyanine derivatives: effect of zn-o coordination bond on morphology and handedness of nanostructures. ChemPhysChem 14:3827–3833

[39] Zhang XF, Xi Q, Zhao J (2010) Fluorescent and triplet state photoactive J-type phthalocyanines nano assemblies: controlled formation and photo snesitizing properties. J Mater Chem 20:6726–6733

[40] Morisue M, Morita T, Kuroda Y (2010) Ligand-assisted J-type aggregates of zinc porphyrin: anticooperative molecular organization in self-assembled bolaamphiphile. Org Biomol Chem 8:3457–3463

[41] Adachi K, Watarai H (2005) Interfacial aggregation of thioether-substituted phthalocyaninatomagnesium(II)-palladium(II) complexes in the toluene/water system. J Mater Chem 15:4701–4710

[42] Geng J, Zhu Z, Qin W et al (2014) Near-infrared fluorescence amplified organic nanoparticles with aggregation-induced emission characteristics for in vivo imaging. Nanoscale 6:939–945

[43] Jang K, Kinyanjui JM, Hatchett DW, Lee DC (2009) Morphological Control of One-Dimensional Nanostructures of T-Shaped Asymmetric Bisphenazine. Chem Mater 21:2070–2076

[44] Cornil J, Beljonne D, Calbert JP, Brédas JL (2001) Interchain interactions in organic π-conjugated materials: impact on electronic structure, optical response, and charge transport. Adv Mater 13:1053–1067